Superhydrophobic nanoparticles: an efficiently selective adsorbent for surfactant-like contaminants from complex wastewater matrices

Lingyue Zhang [a,b], Chuyang Y. Tang [b], Chu Tang [a], Huijing Wang [a], Jianchao Wang [c], Ruiying Li [b], Haopeng Feng [b], Dongbei Yue [a,*]

a School of Environment, Tsinghua University, Beijing 100084, China
b Department of Civil Engineering, The University of Hong Kong, Pokfulam, Hong Kong SAR, China
c School of Chemical and Environmental Engineering, China University of Mining and Technology (Beijing), Beijing 100083, China

Keywords: Superhydrophobic; Selective adsorption; Polydopamine; Hydrophobic interaction; Leachate treatment

Abstract: Surfactant-like contaminants (SLCs) with distinctive amphiphilic structures have become a global concern in wastewater due to their toxicity and persistency. Despite extensive efforts, achieving efficient and selective SLCs removal remains challenging because of their wide range of molecular weights and complex functional group compositions. Superhydrophobic nanoparticles could potentially tackle this challenge by targeting the long oleophilic chains of SLCs. However, conventional contact angle measurements hinder hydrophobicity characterization and corresponding selectivity research because of the powder morphology of nanoparticles. Herein, we offered information regarding the distribution of water molecular probes in surfaces and proposed a quantitative characterization approach based on low-field nuclear magnetic resonance. Through synthesizing superhydrophobic and hydrophilic polydopamine nanospheres with similar morphologies, we systematically demonstrate the selective adsorption potential of superhydrophobic nanoparticles for SLCs. As revealed by the interaction mechanisms, the superhydrophobic surface of nanospheres increased its affinity and selectivity for SLCs adsorption by enhancing hydrophobic interactions. Superhydrophobic modification achieved 10 times the adsorption capacity of sodium dodecyl benzene sulfonate, an exemplified surfactant, compared to pristine nanoparticles. By regulated self-polymerization, the superhydrophobic nanospheres were coated onto the surface of a 3D sponge and enabled efficient selective SLCs adsorption from highly polluted leachate matrices with long-term stability and reusability.

1. Introduction

Surfactants and surface-active agents are frequently used in households and industries[1], and the majority of them are discharged into the environment as detergents and solubilizers[2], particularly in water bodies[3]. Since perfluorooctane sulfonate (PFOS) was listed as a persistent organic pollutant (POP) in 2009[4], surfactant-like contaminants (SLCs) with both hydrophilic (polar) and hydrophobic (lipophilic) portions have aroused broad concern in the field of wastewater treatment owing to their direct and indirect detrimental environmental effects[5]. Their distinctive amphiphilic and accumulation properties[6] are known to cause severe biological toxicity [7], pollutant solubilization, and water eutrophication.

Activated sludge and nanofiltration are the mainstream treatment methods for practical applications with high removal rates and economic costs[8]. Over the past decade, numerous materials, including activated carbon[9], graphene[10], montmorillonit [11], and nano-iron oxide[12], have been proposed for the efficient adsorption or degradation of SLCs in wastewater. However, limited research has focused on the selective removal of SLCs and their related mechanisms owing to the wide range of molecular weights and various functional groups. Previous studies have confirmed that the non-selectivity of current methods significantly reduce the removal efficiency of SLCs in contaminated water by competitive effects and disordered packing[6, 13]. Mixed concentrates and extracts from reported membranes and materials have also been confronted with the inevitable difficulty of recycling and detoxification[1].

Superhydrophobic materials possess surfaces with high apparent contact angles (> 150°), low sliding angles (< 5°)[14], and high stability of Cassie model state[15] has been commonly applied in anti-wetting, oil collection, and oil/water separation because of their low surface energy[16]. In an oil/water separation system[17], oil droplets can thoroughly spread and permeate the superhydrophobic membrane under either a small applied pressure (< 0.3 bar) or gravity[18]. With a three-dimensional structure, superhydrophobic sponges can absorb oil several times their weight[19], which could be a potential material for selective SLCs removal. However, limited studies have been conducted on the potential of superhydrophobic nanoparticles for contaminant removal from sewage, even though hydrophobic interactions have been proven to be a significant factor in organic adsorption[6]. This is related to the lack of quantitative hydrophobicity characterization of powder nanomaterials and understanding of the interaction mechanisms[20]. As extensively reported in previous studies, it is difficult to achieve a uniform surface after tableting the nanopowder, which is affected by rigidity, fluidity, and lubricity[21]. The powder may creep up the side of the liquid droplet, and the liquid may distort the powder surface as well [20]. As shown in Fig. S1, the water contact angle of the powdered carbon nanotubes, which is a typical hydrophobic material, is less than 90°, which is inconsistent with the actual hydrophobic properties.

This present study aims to elucidate the interaction mechanisms between superhydrophobic nanoparticles and contaminants and achieve efficiently selective

SLCs removal. Since Messersmith *et al.* first revealed polydopamine (PDA) as polymer coating in 2007[22], PDA has garnered considerable attention due to its unique adhesive properties on solid substrates. Recognizing the advantages of its adhesive performance in recycling and wide application as a versatile coating platform, we synthesized polydopamine nanospheres (SPDA) with and without superhydrophobic modification based on the Michael addition reaction to systematically demonstrate the indispensable potential of superhydrophobic nanoparticles for efficient and selective SLCs removal. The surface hydrophobicity and water distribution of the powdered materials were innovatively quantified using low-field nuclear magnetic resonance (LF-NMR). Enhanced hydrophobic interactions improve the adsorption affinity and selectivity of SLCs, as confirmed by the isolation of the interaction mechanisms. Furthermore, the proposed superhydrophobic polydopamine nanosphere (S-SPDA) showed self-polymerization and self-adhesiveness properties, indicating extensive application in surface coating and alkali-activated environmental separation materials in highly-polluted wastewater.

2. Results and discussion

2.1. Construction of superhydrophobic nanoparticles and sponge

We report the regulation of surface hydrophobicity by means of Michael addition reaction[23] between the active functional groups of polydopamine and linear alkyl amines. SPDA was first synthesized using a modified oxidative polymerization method. The spherical morphology and nanoparticle diameter (Fig. 1a) were regulated by the optimization of organic phase proportion and substrate concentration (Fig. S3). The superhydrophobic surface was subjected to S-SPDA based on the reduction in surface energy [15]. To explore the practical application performance and solve the key technical difficulties in the recovery and utilization of conventional powder adsorbents, the prepared S-SPDA nanospheres were coated onto a polyurethane sponge (S-SPDA-PU) by manipulating the self-polymerization of dopamine and surface modification (Fig. 1b). Scanning electron microscope (SEM) images (Fig. 1a and Fig. S4) show the consistent nanosphere morphology of the S-SPDA with a diameter of 150–200 nm.

X-ray photoelectron spectroscopy (XPS) and fourier transform infrared (FTIR) characterizations confirmed the proposed chemical reaction (Fig. 1c and Fig. 1d) for synthesizing S-SPDA and S-SPDA-PU. As shown in Fig. 1c, superhydrophobic modification led to a corresponding increase in the relative contents of C and N in S-SPDA and S-SPDA-PU, which is consistent with the chemical structure of octadecylamine. The fitting results of the C 1s peaks (Fig. S5) further demonstrated that the Michael addition reaction increased the relative content of the C-C and C=O functional groups to 77.84% and 5.77%, respectively, on the S-SPDA surface (Table S1) through the introduction of linear alkyl and the generation of negative carbon ions under alkaline conditions. Moreover, as shown in Fig. 1d, the C-H stretching vibration of the alkane-saturated carbon was observed at 2854 cm^{-1} and 2922 cm^{-1} in the FTIR

spectrum of the S-SPDA. The C=C stretching vibration peaks of the SPDA benzene ring at 1406 cm^{-1} were also significantly shifted to 1462 cm^{-1} after surface modification[24], respectively, which is consistent with the predominant Michael addition reaction of the S-SPDA surface.

The superhydrophobic surface modification proposed in this study did not significantly change the morphology of SPDA, which can be verified by both the N_2 adsorption behavior and the pore size distribution. Both S-SPDA and SPDA conform to type-II isotherms (Fig. 1e), indicating that the modified S-SPDA still showed the multilayer reversible adsorption behavior, and the first inflection point is the saturated adsorption capacity of the single molecular layer. In agreement with the SEM results, micropores (< 2 nm) dominated the pore size distribution of SPDA and S-SPDA, which displayed negligible changes in the nanospherical morphology (Fig. 1e). However, the introduction of carbon chains reduces the BET surface while increasing the pore volume of S-SPDA (Table S2).

To avoid the uncertainty caused by the characteristics of powder nanomaterial tableting in contact angle measurements, LF-NMR was innovatively employed in this study to quantify the surface hydrophobicity and molecular dynamics of H_2O confined within the porous matrices. With the application of the Carr–Purcell–Meiboom–Gill multipulse sequence methods (Eq. S1), this study offers a facile methodology to reveal the mechanism regarding the degree of solvent confinement and distribution by multicomponent inversion of the time-domain spectra (Eq. S2). With the application of H_2O as a probe molecule and parameter optimization for nanoparticles (detail conditions shown in Section S1 and Fig. S2), LF-NMR quantitatively demonstrated the T_2 relaxation time of SPDA and S-SPDA to be 950.543 ms and 2409.197 ms, respectively (Fig. 1f). Since the dosage of materials and solvent was identical in SPDA and S-SPDA, the transverse relaxation time (T_2) was positively correlated with the free water content, indicating a significantly improved hydrophobic surface of the S-SPDA. Moreover, an upward shift in the relaxation time as well as enhanced signal intensity was observed from SPDA to S-SPDA. The multicomponent LF-NMR spectrum of SPDA shows a continuous signal at lower relaxation times (~1-80 ms), whereas a limited number of H_2O molecules exist in the sub-nanometer confinement and nanoconfinement domain (0.1-1000 ms) of S-SPDA. As demonstrated in section S1, this water content reduction indicated that the affinity of the surface and micropores of S-SPDA for H_2O molecules was significantly reduced. As the BET surface of SPDA is larger than that of S-SPDA, and there was no significant difference observed in the morphology between SPDA and S-SPDA, we attribute the increase in free water to the hydrophobicity boost that arises from surface energy reduction.

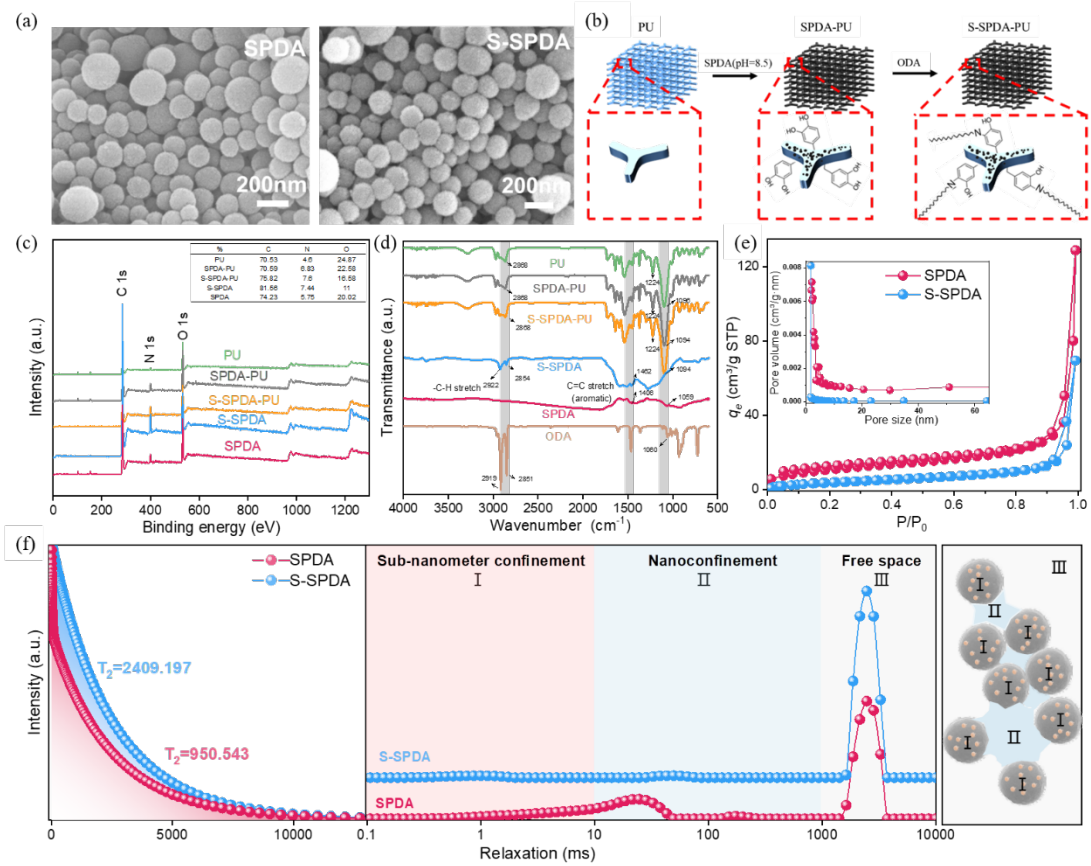

Fig. 1. Fabrication and characterization of superhydrophobic nanospheres. (a) SEM images of SPDA and S-SPDA with a constant spherical structure. (b) Schematic of S-SPDA-PU preparation. XPS patterns (c) and FT-IR spectra (d) of polydopamine nanospheres before and after superhydrophobic modification and the coated sponge. (e) N_2 adsorption–desorption isotherms and pore size distribution. (f) Nuclear magnetic decay curve with the calculated T_2 value and multicomponent inversion of time-domain nuclear magnetic resonance spectra of SPDA and S-SPDA with H_2O as the probe molecule. The inset shows the schematic of each confinement.

2.2. Efficient SLCs removal behaviors

The characterization results indicated that the superhydrophobic surfaces were synthesized without significant morphological transformations. We propose that this surface modification provides efficient and selective adsorption of surfactant-like contaminants with limited influencing variables for mechanism elaboration. To investigate this hypothesis and the adsorption mechanism, sodium dodecyl benzene sulfonate (SDBS), a typical anionic surfactant, was selected as exemplary SLCs for kinetic and isotherm fitting. A series of typical SLCs, including conventional and perfluorinated surfactants, were also conducted for the transverse comparison of different adsorption mechanisms. The detailed properties of the selected pollutants were listed in Table S3.

As shown in Fig. 2a and Table S4, the kinetic data for SPDA and S-SPDA were fitted to the pseudo-second-order kinetic model with a higher correlation coefficient (≥ 0.902).

According to the fitting results, more than 50% of equilibrium adsorption capacity (q_e) was reached within 5 min for S-SPDA with an enhanced adsorption capacity. By calculating the initial adsorption rate (Eq. 3), the S-SPDA and SPDA reached 2.88 mg/(g·min) and 0.23 mg/(g·min) on SDBS adsorption, respectively. This 10 times increase in adsorption rate indicates that the superhydrophobic surface is positively correlated with the adsorption affinity of SDBS, which is attributed to the hydrophobic interaction between the low-surface-energy functional groups. The fitting results of the intraparticle diffusion model (Fig. 2b) further supported this hypothesis. As the fitted curve of the adsorbate does not pass through the origin, diffusion within the particle is not the only step controlling the S-SPDA adsorption process[25]. The Weber-Morris model fitting results indicate that the adsorption process can be divided into two steps:1) the contaminants diffused from the solution to the surface of S-SPDA with a high diffusion rate constant and low mass transfer resistance; 2) the contaminant molecules further diffused from the surface of S-SPDA to the interior of the particles with a relatively low diffusion rate constant, which was mainly affected by steric hindrance. Compared with the fitting results of SPDA, the diffusion rates of SDBS from the solution to the S-SPDA solid surface and intraparticle were significantly increased, indicating that the mass transfer resistance and steric hindrance of the adsorbate subjected to superhydrophobic modification were significantly reduced. As the BET surface area of S-SPDA reduced after superhydrophobic modification (Fig. 1e), this result further proves that the surface superhydrophobic property is the main factor influencing the adsorption enhancement of S-SPDA on SDBS.

The adsorption isotherms of SDBS on SPDA and S-SPDA (Fig. 2e and Table S5) are well described by the Freundlich model, as indicated by the high R^2 (0.967 and 0.905). In agreement with the kinetic results, S-SPDA exhibited a higher adsorption affinity (K_f) than SPDA based on a heterogeneous adsorption process. The K_f of S-SPDA increased from 2.03 to 10.23, indicating that SDBS tends to be adsorbed by the superhydrophobic surface. Furthermore, the results of the Langmuir isothermal model fitting showed that the maximum adsorption capacity of S-SPDA for SDBS was improved as well. The maximum adsorption capacity of SDBS on S-SPDA and SPDA is 146.97 mg/g and 14.11 mg/g, respectively. Similar enhanced adsorption behaviors have been widely observed for other SLCs (Fig. 2e), with the indispensable selectivity of S-SPDA for the octanol-water partition coefficient (logP value). Overall, superhydrophobic surfaces enable highly efficient SLCs removal with an enhanced adsorption affinity and a higher initial adsorption rate than previously reported adsorbent materials[6].

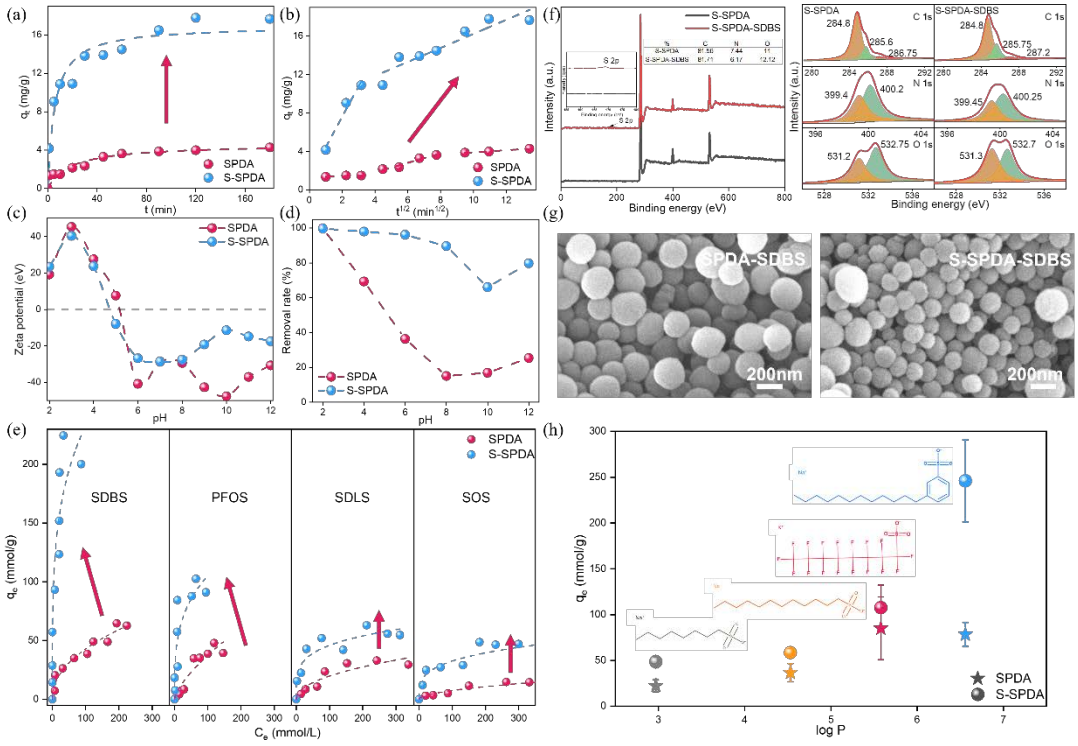

Fig. 2. Adsorption behaviors of superhydrophobic nanospheres and selective mechanism elucidation. (a) Adsorption kinetic and fitting results of pseudo-second-order model. (b) Intraparticle diffusion for the adsorption of SDBS. The initial concentration of SDBS is 20 mg/L. (c) The ζ-potential of SPDA and S-SPDA as a function of pH. (d) Effects of pH value on SDBS adsorption. (e) Isotherm and fitting results of Freundlich model on SLCs adsorption. (f) XPS spectrum, C 1s core region, N 1s core region, and O 1s core region of S-SPDA before and after SDBS adsorption. (g) SEM images of SPDA and S-SPDA after SDBS adsorption. (h) Maximum adsorption capacities of SPDA and S-SPDA on SLCs with logP variation.

2.3 Mechanisms of selective SLCs removal

These adsorption results demonstrate that superhydrophobic modification significantly improves the adsorption capability of SLCs. To better analyze the selectivity and its mechanism, the effects of pH value on ζ-potential and SLCs removal rate were first investigated. As shown in Fig. 2c, the isoelectric pH of S-SPDA (pH = 4.73) decreased slightly compared to that of SPDA (pH = 5.00), which was attributed to the enhanced electronegativity of the acidic functional groups on the S-SPDA surface after the addition reaction of the modifier. This agrees with the tendency of the adsorption removal rate to be influenced by the pH value. For example, both SPDA and S-SPDA showed a downward trend in SDBS removal with an increase in pH value, whereas the decline in S-SPDA was relatively limited (Fig. 2d). Since the p*K*a of SDBS is 0.7, the surfaces of the adsorbents and SDBS are both negatively charged when the pH value is larger than the isoelectric point (IEP), resulting in increased electrostatic repulsion and inhibited adsorption quantity. A similar trend was observed for the

hydrogen bond interactions between the adsorbents and SDBS. When the pH value of the system increased, the sulfonic group ionization of SDBS was negligibly affected, while the phenol hydroxyl ionization in the polyamine was enhanced, resulting in a relatively weak hydrogen bond. Simultaneously, the amino group in the benzene ring structure of S-SPDA is gradually deprotonated, which reduces the content of hydrogen protons participating in hydrogen bonding. Therefore, the decrease in the adsorption capacity of biomimetic polydopamine nanomaterials is attributed to both electrostatic and hydrogen bond interactions. However, the high removal rate (74.33%) at pH 12 demonstrates that the influence of these interactions on S-SPDA was far less than that of SPDA.

The XPS spectrum (Fig. 2f) shows that SDBS adsorption increased the relative content of oxygen and sulfur elements, whereas the composition of the functional groups of each element did not change significantly. The morphologies of the SPDA and S-SPDA were consistent before and after adsorption (Fig. 2g). Their characterization results indicated that SDBS is mainly physically adsorbed on the S-SPDA surface, and there is no significant change in the chemical bond and material morphology. Therefore, to explore the selective mechanism of S-SPDA and realize the isolation between different interactions, a series of characteristic organic compounds was selected for comparison with the molar adsorption capacity to avoid the effects of molecular weight. The system pH was adjusted to the IEP of S-SPDA and SPDA to reduce the influence of electrostatic interactions.

Since SDBS with a sulfonic group act as an electron acceptor in the interaction with the π-π electron donor-acceptor of S-SPDA, the introduction of the long carbon chain after the superhydrophobic modification enhances the electron cloud density of the benzene ring in the SPDA structure, thus promoting π–π electron donor-acceptor interactions. Therefore, the adsorption results of SLCs, including sodium dodecyl sulfonate (SDLS), sodium 1-octane sulfonate (SOS), and potassium perfluorooctyl sulfonate (PFOS), with a similar structure and no benzene ring were significant supplements for further comparison of π – π and hydrophobic interactions (Fig. 2e). Under the pH value at the IEP, the lack of a benzene ring and the sharp decrease in hydrophobicity resulted in the limited adsorption capacity of S-SPDA on SDLS, but the maximum adsorption capacity of S-SPDA material for PFOS (107.48 mmol/g) is much higher than that of SDLS (58.45 mmol/g) and SOS (48.62 mmol/g), which is attributed to the critical difference between the fatty chain and the perfluorocarbon chain with higher hydrophobicity. Moreover, S-SPDA showed indispensable selectivity for the logP value of the adsorbate (Fig. 2h) with an enhanced maximum adsorption capacity and larger K_f. The difference of adsorption properties between S-SPDS and SPDA also enlarged with the increase of logP value. By comparing adsorption isotherm of SPDA and S-SPDA, the difference between S-SPDA and SPDA in adsorption efficiency and selectivity extensively enlarged in the adsorption of pollutants with higher logP values. As illustrated in Figures 1f, 2d, and 2e, the substantial difference in adsorption selectivity, resulting from the transformation of surface and pore channels from

hydrophilic to superhydrophobic, is more prominent than the changes in electrostatic interaction caused by minor variations in functional groups or system pH.

These comparative results suggest that hydrophobic interactions play a crucial role in the adsorption mechanism. Consequently, enhanced hydrophobic interactions enable superhydrophobic materials to display robust selective adsorption capability for SLCs possessing amphiphilic properties in aqueous systems.

2.4 Selective removal performance in complex wastewater matrices

The constant superhydrophobic surface and adsorption mechanism proposed in this study make it possible for selective adsorption to remove SLCs. As shown in Fig. 1b, S-SPDA-PU was used to further investigate the selectivity and utilization performance in contaminated wastewater. SEM images (Fig. S4) confirmed a nanosphere layer with a diameter of 150–200 nm, aligned with the morphology of SPDA and S-SPDA on the smooth surface of the PU sponge in SPDA-PU and S-SPDA-PU, respectively. In agreement with the LF-NMR results, the TrueDrop method was applied to collect water contact angles from the PU, SPDA-PU, and S-SPDA-PU sponges, and showed that the water contact angle was transferred from 120° of the original PU sponge to 55° and 155° with the SPDA and S-SPDA coatings (Fig. 3a), respectively. As shown in Fig. 3b, a water droplet was sufficiently contacted and completely lifted onto the surface of S-SPDA-PU. This was consistent with the outstanding water-repellent characteristics of the S-SPDA surface. More than that, the superhydrophobic property of the S-SPDA-PU surface was relatively stable under extreme test conditions, including strong acid (pH = 1), strong alkali (pH = 13), saturated NaCl, 200℃, and -18 ℃ for 48 h (Fig. S6). This was attributed to the strong covalent and noncovalent interactions between the S-SPDA and the PU substrate[22]. The enhanced SLCs adsorption performance of S-SPDA-PU, shown in Fig. 3c and Table S6 (SDBS for example), was consistent with that of S-SPDA. The adsorption equilibrium was reached within 10 min with a 10 times removal rate than of SPDA-PU and PU.

To further demonstrate the SLCs selective adsorption performance in complex wastewater matrices, municipal solid waste (MSW) leachate containing much higher organic[26] (The concentration of total organic carbon (TOC) is ranging from 3000 mg/L to 10000 mg/L) and salt concentrations (The concentration of total dissolved solids is ranging from 10000 mg/L to 30000 mg/L) than domestic sewage[27] was sampled from 6 leachate treatment plants in this study. Representative cationic and nonionic surfactants were quantified as well within the leachate before and after adsorption to comprehensively verify the selective SLCs adsorption ability of S-SPDA-PU. At a 1/10 volume ratio of sponge to leachate, the concentration of total SLCs in the leachate at different landfill ages[28] decreased significantly after adsorption (Fig. 3d). Compared to commercial nanofiltration processes[8] and state-of-the-art research absorbents[2, 6], S-SPDA-PU exhibited high selectivity for the removal of anionic, cationic, and nonionic SLCs in practical contaminated wastewater, reaching up to 81.88% of the total SLCs removal rate of MSW leachates. Despite extremely high concentration of organic

pollutants and salts in aged leachate, which was widely regarded as a highly complex wastewater system, S-SPDA-PU achieved a selective SLCs removal efficiency of average 69.28%. It is worth noting that the concentration of most SLCs was less than 0.050 mg/L in the sampled leachate, whereas the concentration of TOC was greater than 3000 mg/L. This indicates that S-SPDA-PU selectively adsorbed micro or trace SLCs in complex wastewater, which is expected because of the long hydrophobic chains of the SLCs that interact with the superhydrophobic surface.

Since hydrophobic interactions dominate the adsorption process of SLCs on S-SPDA-PU, an economical and less side-effect desorption method using ethanol as an example was proposed in this study. Shielded hydrophobic interactions effectively released SLCs from the adsorbent with a desorption rate of 90.27% (Fig. S7) and resumed after drying. After four reuse cycles, the adsorption and desorption rates of S-SPDA-PU decreased by only 1.50% and 2.28%, respectively (Fig. 3e and Table S7), demonstrating a comparable reusability. Moreover, after 10000 times of mechanical extrusion (Fig. 3f), the height of the original PU sponge decreased from 2 cm to 1.8 cm, whereas the height of S-SPDA-PU remained at 2 cm with a constant superhydrophobic surface (water contact angle = 153°, Fig. 3g). The test results showed that the S-SPDA coating improved the mechanical stability of PU and resulted in a more durable reuse potential, attributing to the mechanical reinforcing effect of S-SPDA nanoparticles anchored on the interconnected skeleton[29]. Based on the direct SLCs removal efficiency in complex wastewater matrices and practical properties, our studies drew a new paradigm (Fig. S8) to supply S-SPDA-PU as pretreatment process to targeted removal of trace SLCs from wastewater.

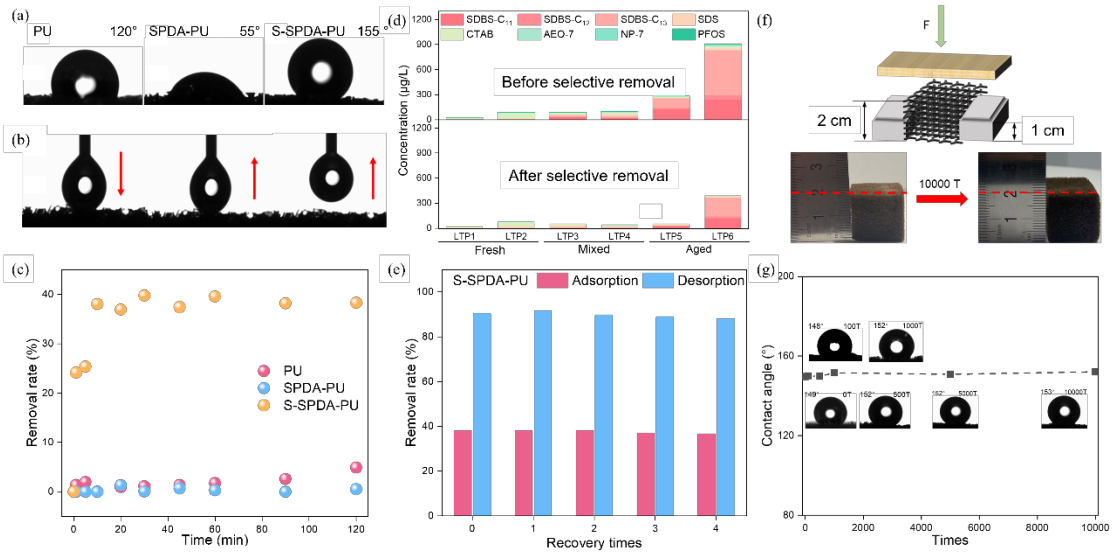

Fig. 3. Selective SLCs adsorption and application performance of superhydrophobic nanospheres coated sponge in sampled MSW leachate. (a) Water contact angle of original PU, SPDA-PU, and S-SPDA-PU. (b) The dynamic adhesion test results of water droplet on S-SPDA-PU. (c) SDBS removal rate over time for original PU, SPDA-PU, and S-SPDA-PU. (d) The concentration of SLCs in 6 sampled MSW leachate before and after selective adsorption of S-SPDA-PU. (e) SDBS adsorption and

desorption rate of S-SPDA-PU over 4 times reusing. The initial concentration of SDBS in (c) and (e) is 20 mg/L. (f) Schematic of mechanical test and digital photograph of S-SPDA-PU after 10000 times presses. (g) Negligible effects of mechanical press on the water contact angle of S-SPDA-PU.

3. Conclusions

Owing to the lack of separation and comparison between adsorption interactions, current adsorption materials have difficulty achieving high selectivity for SLCs, while other superwetting materials concentrate on the separation of oil and water phases instead of aqueous systems.

In this study, we fabricated superhydrophobic dopamine nanospheres and coated them onto the surface of a PU sponge for selective SLCs adsorption. Based on T_2 relaxation time, the surface hydrophobicity of powder nanoparticles and the distribution of water molecular probes was innovatively quantified. As elucidated by interaction mechanisms, the dominant role of hydrophobic interaction in the adsorption of S-SPDA enabled efficient SLCs removal and high selectivity even in complex contaminated leachate matrices. Moreover, S-SPDA adhered to the PU surface without adding extra adhesive, thereby avoiding secondary toxicity and recovery of the powder materials. Desorption methods for shielding hydrophobic interactions reduce the cost of recycling and enhance the durability of adsorbents.

Our study provides valuable insights and feasible strategy for quantifying the surface hydrophobicity of powder nanoparticles and extends their potential use in the elucidation of interaction mechanisms between nanoparticles and contaminants. Compared to previously reported adsorption materials and commercial membranes, S-SPDA-PU, which has a stable superhydrophobic surface and practical reusability, shows high efficiency and selectivity for the removal of SLCs. This creates potential for the application of superhydrophobic sponges in the selective removal of SLCs from wastewater as pretreatment process.

4. Experimental Section

Materials

Hydrochloric acid (HCl, 36-38%), sodium hydroxide (NaOH, > 98%), and ammonium acetate (LC/MS grade, > 99%) were purchased from Sigma-Aldrich (Shanghai, China). Methanol (HPLC grade, 99.9%) was purchased from Fisher Chemical (Leicestershire, England). Dopamine hydrochloride ($C_8H_{11}NO_2$·HCl, 98%), sodium dodecyl benzene sulfonate standard solution (SDBS, $C_{18}H_{29}SO_3Na$, analytical standard grade), sodium dodecyl sulfonate (SDLS, $C_{12}H_{25}SO_3Na$, ≥ 99.0%), sodium octane sulfonate (SOS, $C_8H_{17}SO_3Na$, ≥ 99.0%), nonylphenol ethoxylate (NP-7, $C_{15}H_{24}O(C_2H_4O)_7$, AR), fatty alcohol polyoxyethylene ether (AEO-7, $RO(CH_2CH_2O)_7H$, AR), cetyl trimethyl ammonium bromide (CTAB, $C_{19}H_{42}BrN$, ≥

99.0%) and tris hydrochloric acid buffer (Tris, pH = 8.5) were purchased from Aladdin (Shanghai, China). Potassium perfluorooctyl sulfonate (PFOS, $C_8F_{17}SO_3K$, > 98%) was purchased from Merida (Beijing, China). Octadecyl amine ($C_{18}H_{39}N$, analytical reagent) was purchased from Anergic (Shanghai, China), anhydrous ethanol (C_2H_6O, > 99.7%) was purchased from Titan (Shanghai, China). Polyurethane sponges (PU) were purchased from Yongjia Sponge Products Co., Ltd. The ultrapure water used to prepare the solution is prepared by Master-S UV ultrapure water machine.

Adsorbent preparation

SPDA was synthesized by increasing the proportion of organic phase in solvent system. Dopamine of different quality was dissolved in a mixed solution of 20% (v/v) ethanol and Tris-HCl buffer solution (pH = 8.5, 10 mmol/L), and was fully mixed with a magnetic stirrer under dark at room temperature for 24 hours. The resulting solution was centrifuged at 13000 rpm for 10 min and the obtained product was rinsed three times with ethanol and ultrapure water. The resulting precipitate was collected and freeze-dried to get SPDA as black powder.

The synthesis procedure for S-SPDA was as follows: A ethanol solution (100 mL) containing the prepared SPDA nanomaterials (10 mg) and octadecyl amine (269.51mg) were stirred at 60℃ for 12 hours with a magnetic stirrer. The resulting reaction mixture was centrifuged at 13000 rpm for 10 min and rinsed three times with ethanol. The obtained precipitate was freeze-dried and denoted as S-SPDA.

S-SPDA was further coated on the surface of the PU porous-sponge for environmental application. PU (1 cm × 1 cm × 1cm) was ultrasonically cleaned with ethanol and ultrapure water and dried at 60℃. The obtained PU was added into the above SPDA and S-SPDA reaction mixture in turn and was fully rinsed with water and ethanol for more than ten times. After rinse process, no nanoparticles were observed in the effluent solution. The resulting black sponge was freeze-dried and denoted as SPDA-PU and S-SPDA-PU, respectively.

Batch adsorption experiment

Adsorption experiments were conducted using a batch approach at ambient temperature. To initiate the experiment, absorbent (200 mg) was added into 200 mL of surfactant-like pollutants solution with a series of initial concentrations (5–100 mg/L). With 200 rpm stirring, samples were taken in a certain time and adsorption equilibrium (24h) for adsorption kinetics and isotherms, respectively. pH was adjusted using 0.1 M NaOH and 0.1 M HCl and monitored by pH meter (T50, Mettler Toledo, Switzerland). All adsorption experiments were run in duplicate.

After filtration through 0.22 μm membranes, quantitative analysis of samples was performed on Acquity UPLC (Waters, USA) coupled with a Xevo TQD (Waters, United States) triple quadrupole tandem mass spectrometry (MS/MS). The detailed optimization methods were developed in our previous study [30]. Briefly, gradient elution was conducted using 5 mM ammonium acetate and 0.5% (v/v) formic acid in water (A) and methanol (B) with a BEH-C18 column (1.7 μm, 2.1 × 100 mm, Waters, USA). Electrospray ionization (ESI) source and negative multi-reaction monitoring

(MRM) mode were adopted in MS/MS. The post-column compensation method was applied and optimized to improve the detection limit with 30 μL/min of 10% ammonium hydroxide in water. The specific gradient elution conditions and corresponding mass spectrum conditions of each surfactant were listed in Table S8 and S9.

The pseudo-first-order (Eq. 1) and pseudo-second-order model (Eq. 2) was applied to fit the adsorption data of kinetic studies.

$$q_t = q_e(1 - e^{-k_1 t}) \tag{1}$$

$$q_t = \frac{q_e^2 k_2 t}{1 + q_e k_2 t} \tag{2}$$

where q_t (mg/g) is the adsorption amounts of pollutants at time t (min), q_e (mg/g) is the adsorption amounts of pollutants at equilibrium time, and k_1 (mg/(g·min)) and k_2 (g/(mg·min)) is the rate constant. According to Eq. 2, initial adsorption rate was calculated as Eq. 3:

$$v_0 = q_e^2 k_2 \tag{3}$$

where v_0 (mg/(g·min)) is the initial adsorption rate. The diffusion mechanisms were conducted by fitting the intraparticle diffusion model (Eq. 4).

$$q_e = k_{id} t^{1/2} + C \tag{4}$$

where k_{id} (mg·min$^{1/2}$/g) is the interparticle diffusion rate constant and C (mg/g) is the boundary layer thickness constant. The adsorption isotherms were simulated by the Freundlich model (Eq. 5).

$$q_e = K_f C_e^{\frac{1}{n}} \tag{5}$$

where C_e (mg/L) is the concentration of residual pollutants in solution at equilibrium, and K_f (mg·(L/mg)$^{1/n}$/g) and n are the constant of the Freundlich model.

Environmental application experiment

Application adsorption experiments were conducted using a batch approach at ambient temperature. To initiate the experiment, original and coated PU (1 cm × 1 cm × 1cm) was added into 50 mL of surfactant-like pollutants solution with an initial concentration (20 mg/L). With 200 rpm stirring, samples were taken in a certain time and adsorption equilibrium (24h) for adsorption kinetics and isotherms, respectively. The removal rate of original and coated PU was calculated as Eq.6:

$$\text{Removal rate}(\%) = \frac{C_0 - C_t}{C_0} \times 100\% \tag{6}$$

where C_0 (mg/L) is the initial concentration of pollutants and C_t (mg/L) is the residual concentration of pollutants at time t (min).

Ethanol was used as an exemplary desorption agent. First, the adsorbed powder

materials were centrifuged for 10 min at 130000 rpm and desorbed for 2 hours at ambient temperature. After desorption, the obtained materials were washed 3 times with ultrapure water. As for sponge materials, the adsorbed sponge was first fully squeezed to discharge the adsorbed solution and immersed in ethanol for 2 hours at ambient temperature. Reusing experiments were conducted with the same SDBS concentration (20 mg/L) and materials dosage (20 mg for S-SPDA and 1 cm × 1 cm × 1cm for S-SPDA-PU into 50 mL solution, respectively) as adsorption experiment. The eluent was set as 50 mL and cautiously collected. Since the volume of adsorption solution and eluent are same, the desorption rate was calculated as:

$$\text{Desorption rate}(\%) = \frac{C_d}{C_0 - C_e} \times 100\% \quad (7)$$

where C_d (mg/L) is the concentration of eluent collected after desorption.

To perform the selectivity in complex wastewater matrices, this study collected leachate samples from 6 typical MSW landfills and waste-to-energy plants. It is noteworthy that landfill ages from fresh to aged were all included in these samples. A description of the characteristics of all leachate samples and extraction methods were detailed listed in previous study[30]. Briefly, each sample was filtered by a 0.45 μm membrane before solid phase extraction (SPE) and quantified with UPLC/MS/MS.

Characterization

The morphology of adsorbents was observed by scanning electron microscope (SEM) with a Hitachi SU-8010. Fourier transform infrared (FTIR) spectra were measured to determine chemical groups using a Bruker Vertex 70 with the range of 350 cm^{-1}– 4000 cm^{-1}. The Brunauer-Emmett-Teller (BET) and Barrett-Joyner-Halenda (BJH) equations were used to calculate the surface area and pore size destitution with a Quantachrome SI-MP. X-ray photoelectron spectroscopy (XPS) spectra was record in a Thermo ESCALAB 250XI to determine surface elemental composition and valency. The zeta potential was measured with Zeta potentiometer (Delsa Nano C, Beckman Coulter). It is worth noting that the hydrophilicity and water distribution characteristics of adsorbents were innovatively quantified by LF-NMR with VTMR20-010V-I at about 0.5 T of main magnetic field. Detailed characterization mechanism and methods were described in Section S1.

Statistical Analysis

The results were reported as mean ± standard deviation (SD).

Supporting Information

Supporting Information is available from the Wiley Online Library or from the author.

Acknowledgements

This study was funded by the National Key Research and Development Program of China (2018YFC1901405). Special thanks go to Dr. Haijun Yang and Hao Ding for

their professional support in the characterization with Low field nuclear magnetic resonance.

Conflict of Interests

The authors declare no conflict of interest.

Data Availability Statement

The data that support the findings of this study are available from the corresponding author upon reasonable request.

Keywords

Superhydrophobic; Selective adsorption; Polydopamine; Hydrophobic interaction; Leachate treatment

References

[1] M. Palmer, H. Hatley, *Water Res.* **2018**, 147, 60.
[2] R. F. Nunes, A. C. S. C. Teixeira, *Chemosphere* **2022**, 300, 134507.
[3] N. Sakai, J. Shirasaka, Y. Matsui, M. R. Ramli, K. Yoshida, M. A. Mohd, M. Yoneda, *Chemosphere* **2016**, 172, 234.
[4] C. Gallen, D. Drage, G. Eaglesham, S. Grant, M. Bowman, J. F. Mueller, *J. Hazard. Mater.* **2017**, 331, 132.
[5] J. Arora, A. Ranjan, A. Chauhan, R. Biswas, V. D. Rajput, S. Sushkova, S. Mandzhieva, T. Minkina, T. Jindal, *J. Appl. Microbiol.* **2022**, 133, 1229.
[6] A. A. Siyal, M. R. Shamsuddin, A. Low, N. E. Rabat, *J. Environ. Manage.* **2020**, 254, 109797.
[7] M. Lechuga, M. Fernandez-Serrano, E. Jurado, J. Nunez-Olea, F. Rios, *Ecotoxicol. Environ. Saf.* **2016**, 125, 1.
[8] F.-J. Zhu, W.-L. Ma, T.-F. Xu, Y. Ding, X. Zhao, W.-L. Li, L.-Y. Liu, W.-W. Song, Y.-F. Li, Z.-F. Zhang, *Ecotoxicology and Environmental Safety* **2018**, 153, 84.
[9] M. Bautista-Toledo, J. Méndez-Díaz, M. Sánchez-Polo, J. Rivera-Utrilla, M. Ferro-García, *J. Colloid Interface Sci.* **2008**, 317, 11.
[10] P. Prediger, T. Cheminski, T. de Figueiredo Neves, W. B. Nunes, L. Sabino, C. S. F. Picone, R. L. Oliveira, C. R. D. Correia, *J. Environ. Chem. Eng.* **2018**, 6, 1536.
[11] M. J. Sánchez-Martín, M. C. Dorado, C. del Hoyo, M. S. Rodríguez-Cruz, *J. Hazard. Mater.* **2008**, 150, 115.
[12] C. C. Borghi, M. Fabbri, M. Fiorini, M. Mancini, P. L. Ribani, *Sep. Purif. Technol.* **2011**, 83, 180.
[13] Q. Gao, W. Chen, Y. Chen, D. Werner, G. Cornelissen, B. Xing, S. Tao, X. Wang, *Water Res.* **2016**, 106, 531.

[14] A. A. Alazab, T. A. Saleh, *Mater. Chem. Phys.* **2023**, 302, 127609.
[15] J. Jeevahan, M. Chandrasekaran, G. Britto Joseph, R. B. Durairaj, G. Mageshwaran, *J. Coat. Technol. Res.* **2018**, 15, 231.
[16] M. Nosonovsky, B. Bhushan, *Curr Opin Colloid Interface Sci* **2009**, 14, 270.
[17] M. Satria, T. A. Saleh, *J. Mol. Liq.* **2022**, 367, 120341.
[18] L. Wen, Y. Tian, L. Jiang, *Angew. Chem. Int. Ed.* **2015**, 54, 3387.
[19] H. Wang, J. Yang, X. Liu, Z. Tao, Z. Wang, R. Yue, *J. Mater. Sci.* **2019**, 54, 1255.
[20] A. Alghunaim, S. Kirdponpattara, B.-m. Z. Newby, *Powder Technol.* **2016**, 287, 201.
[21] A. Depalo, A. C. Santomaso, *Colloids Surf., A* **2013**, 436, 371.
[22] H. Lee, S. M. Dellatore, W. M. Miller, P. B. J. s. Messersmith, *Science* **2007**, 318, 426.
[23] M. Ghasemlou, F. Daver, E. P. Ivanova, B. J. J. o. M. C. A. Adhikari, *J. Mater. Chem. A* **2019**, 7, 16643.
[24] T. A. Saleh, *Chem. Eng. J.* **2021**, 404, 126987.
[25] N. F. Campos, C. M. B. M. Barbosa, J. M. Rodríguez-Díaz, M. M. M. B. Duarte, *Adsorp Sci Technol* **2018**, 36, 1405.
[26] L. Zhang, M. C. Lavagnolo, H. Bai, A. Pivato, R. Raga, D. Yue, *Resources, Conservation and Recycling* **2019**, 141, 474.
[27] L. Zhang, X. Wang, D. Yue, *Environmental Pollution* **2020**, 267, 115573.
[28] L. Zhang, H. Bai, Y. Zhang, Y. Wang, D. Yue, *Environmental Science & Technology* **2021**, 55, 13264.
[29] H. Wang, E. Wang, Z. Liu, D. Gao, R. Yuan, L. Sun, Y. Zhu, *J. Mater. Chem. A* **2015**, 3, 266.
[30] L. Zhang, C. Tang, M. Li, H. Wang, S. Zhang, J. Wang, X. Dong, D. Fang, H. Bai, Y. Sun, D. Yue, *Water Res.* **2023**, 231, 119487.